Available online at www.sciencedirect.com
SCIENCE DIRECT®
Icarus 168 (2004) 420–432
ICARUS
www.elsevier.com/locate/icarus

Catastrophic disruption of pre-shattered parent bodies

Patrick Michel,[a,*] Willy Benz,[b] and Derek C. Richardson [c]

[a] *Observatoire de la Côte d'Azur, CNRS/UMR 6202 Cassiopee, Bd de l'Observatoire, B.P. 4229, 06304 Nice cedex 4, France*
[b] *Physikalisches Institut, University Bern, Sidlerstrasse 5, CH-3012 Bern, Switzerland*
[c] *Department of Astronomy, University of Maryland, College Park, MD 20742-2421, USA*

Received 23 August 2003; revised 2 December 2003

Abstract

In this paper, we analyze the effect of the internal structure of a parent body on its fragment properties following its disruption in different impact energy regimes. To simulate an asteroid breakup, we use the same numerical procedure as in our previous studies, i.e., a 3D SPH hydrocode to compute the fragmentation phase and the parallel *N*-body code `pkdgrav` to compute the subsequent gravitational re-accumulation phase. To explore the importance of the internal structure in determining the collisional outcome, we consider two different parent body models: (1) a purely monolithic one and (2) a pre-shattered one which consists of several fragments separated by damaged zones and small voids. We present here simulations spanning two different impact energy regimes—barely disruptive and highly catastrophic—corresponding to the formation of the Eunomia and Koronis families, respectively. As we already found for the intermediate energy regime represented by the Karin family, pre-shattered parent bodies always lead to outcome properties in better agreement with those of real families. In particular, the fragment size distribution obtained by disrupting a monolithic body always contains a large gap between the largest fragment and the next largest ones, whereas it is much more continuous in the case of a pre-shattered parent body. In the latter case, the ejection speeds of large fragments are also higher and a smaller impact energy is generally required to achieve a similar degree of disruption. Hence, unless the internal structure of bodies involved in a collision is known, predicting accurately the outcome is impossible. Interestingly, disrupting a pre-shattered parent body to reproduce the Koronis family yields a fragment size distribution characterized by four almost identical largest objects, as observed in the real family. This peculiar outcome has been found before in laboratory experiments but is obtained for the first time following gravitational re-accumulation. Finally, we show that material belonging to the largest fragments of a family originates from well-defined regions inside the parent body (the extent and location of which are dependent upon internal structure), despite the many gravitational interactions that occur during the re-accumulation process. Hence fragment formation does not proceed stochastically but results directly from the velocity field imparted during the impact.

Keywords: Asteroids, composition; Asteroids, dynamics; Collisional physics; Impact processes

1. Introduction

In this paper, we analyze the effect of the internal structure of a parent body on its fragment properties following disruption in different impact energy regimes. Our recent simulations of the formation of the young Karin family (Michel et al., 2003) in the intermediate energy regime indicated that the disruption of a monolithic parent body does not reproduce the properties of the real family, as determined by Nesvorný et al. (2002). In particular, for a monolithic target, there is always a lack of fragments with sizes comparable to (but smaller than) the largest fragment, whereas the Koronis family, for example, has four such large members. Conversely, the size and orbital distribution of real family members are well reproduced from the disruption of a pre-shattered parent body.

In order to investigate in more detail the effect of the internal structure of the parent body on the collisional outcome in different impact energy regimes, we have simulated the formation of the Eunomia and Koronis families using both a monolithic and a pre-shattered parent body. The Eunomia family represents a collision in a barely disruptive impact regime, whereas the Koronis family was formed in a catastrophic impact regime. The formation of the Eunomia and Koronis families using monolithic parent bodies has been simulated previously (Michel et al., 2001, 2002). However, these simulations used somewhat arbitrary impact

* Corresponding author.
E-mail address: patrick.michel@obs-azur.fr (P. Michel).

0019-1035/$ – see front matter
doi:10.1016/j.icarus.2003.12.011

angles and velocities. Therefore, to allow a direct comparison with the simulations using pre-shattered parent bodies, we redid all the simulations using, for both kinds of parent body models, the same projectile speed (5 km/s), the same set of impact angles (0° and 45°), and the same free parameters that need to be defined. This paper presents the results of all these simulations.

The assumption that large parent bodies are pre-shattered before being disrupted is appropriate not just because it may potentially lead to a closer match with observed properties. The assumed pre-shattered state is thought to be a natural consequence of the collisional evolution of main belt asteroids. Indeed, several studies have indicated that, for any asteroid, collisions at high impact energies leading to dispersal of fragments occur with a smaller frequency than collisions at lower impact energies leading only to disruption without fragment dispersal, i.e., shattering (see, e.g., Richardson et al., 2002; Asphaug et al., 2002). Thus, in general, a typical asteroid gets battered over time until a major collision eventually disperses it as smaller pieces (Melosh and Ryan, 1997). Consequently, since the formation of an asteroid family corresponds to the ultimate disruptive event of a large object, it is reasonable to think that the internal structure of this body has been modified from its primordial state by all the smaller collisional events that it has suffered over its lifetime in the belt.

The battering scenario is also suggested by spacecraft observations of small bodies (Mathilde and Eros by *NEAR Shoemaker*, Ida and Gaspra by *Galileo*) which have shown that fracture features as well as many craters are present on the irregular surfaces of these objects (e.g., Belton et al., 1995; Chapman et al., 1996; Thomas et al., 2000). However, direct determination of the internal structure of a small body has yet to be made and would require a dedicated space mission to an asteroid (although the measured properties would be specific to that object). Until such a mission, any a priori model of internal structure will necessarily be based on assumptions.

Nevertheless, an indirect method can be developed to discriminate between the different possible internal properties of an asteroid family parent body. As we demonstrate here, by simulating the breakup of a family parent body using different models of its internal structure, we can define which among these models provides the best match to the real family. In particular, we will show for the first time that the disruption of a pre-shattered Koronis parent body can explain the provenance of its four largest similar-sized family members, whereas disruption of a monolithic parent body cannot. The actual presence of these members in the real family was previously a matter of debate requiring alternative formation scenarios (see Section 5).

As we have done in the particular case of the Karin family (Michel et al., 2003), we study here two types of parent bodies differing only by their internal structure, either monolithic or pre-shattered. Monolithic parent bodies have an internal structure characterized by a Weibull distribution of incipient flaws (Weibull, 1939), whereas pre-shattered parent bodies initially also contain a set of internal fragments distributed within the body. These models are described in Section 2 and our numerical method is detailed in Section 3. Section 4 summarizes the results in the low impact energy regime represented by the Eunomia family formation. The intermediate regime, represented by the Karin family, has already been studied elsewhere (Michel et al., 2003), but the results will be included in the different tables. Section 5 presents the results for the catastrophic regime represented by the Koronis family. A discussion follows in Section 6, with conclusions in Section 7.

2. Models of pre-shattered parent bodies

A network of fractures inside a parent body resulting from many uncorrelated small impacts is unlikely to yield spherical internal fragments whose sizes follow a well defined power law. To model a pre-shattered target, we have therefore devised an algorithm that distributes a given number of internal fragments of arbitrary shape and size within the volume of the parent body. For this, we first choose the total number of fragments that must be generated. This number of fragment "seed" particles is then selected randomly but uniformly from among the normal particles in the parent body. Next, fragments are grown concurrently one particle at a time by adding a particle at random from the list of all particles neighboring those already in the fragment. Particles that are found to belong to two or more fragments are classified as "fracture" particles and are assigned a damage value of $D = 1$ (totally damaged). The procedure is repeated until all particles are assigned to fragments or to fractures. To avoid having all fragments meet at the center of the body, we force one seed to be initially within $r/R = 0.3$, where R is the radius of the parent body and r is the distance of the seed from the body's center. Finally, void space is created by randomly removing a given number of particles from the fractured set. This algorithm was used by Michel et al. (2003) to create the model of a pre-shattered Karin parent body. As we will show, besides the fact that it constrains the impact energy needed to achieve a given degree of disruption, the internal structure of the parent body also has important consequences on the outcome properties of the collision.

We also built a model of a pre-shattered parent body in which large fragments are preferentially distributed near the center and smaller fragments are generated close to the surface. We performed some simulations using this model but the collisional outcomes did not show any major qualitative difference compared to those obtained from the first model. At our current level of capability, and considering only qualitative differences, we believe that slight changes to the distribution of internal fragments within the target do not give rise to any relevant differences in the outcome. In this paper, we limit ourselves to using the model generated from a uniform distribution of seeds.

Note that the rubble pile model used to simulate the Karin family formation event in Michel et al. (2003) was constructed differently. In that case, spheres whose sizes followed a specified power law distribution were distributed at random inside the parent body. Particles not belonging to a sphere were removed to create void space and particles at the interface of two or more spheres were assigned to fractures. The fragment characteristics (size and speed) obtained with this model are compared to the one obtained using the pre-shattered model described above in Michel et al. (2003). Some outcome properties obtained with this model are also reported here in the different tables. It is shown that both lead to very similar results.

3. Numerical method

We refer the reader to Michel et al. (2001, 2002) for a detailed description of the numerical method used to perform our simulations. Here we just recall that the fragmentation phase is computed using a 3D SPH hydrocode (Benz and Asphaug, 1995, 1999) assuming basalt bodies and the Tillotson equation of state (Tillotson, 1962). Comparison calculations using the ANEOS equation of state (Thompson and Lauson, 1972) have shown that for collisions that do not include significant phase transitions, the details of the equation of state do not matter much.

The gravitational phase is then computed using the parallel N-body code `pkdgrav` (Richardson et al., 2000). This code detects and treats collisions and mergers between particles on the basis of different options that were investigated by Michel et al. (2002) for monolithic parent bodies. Here we use the most realistic treatment in which a criterion based on relative speed and angular momentum is applied: fragments are allowed to merge only if their relative speed is smaller than their mutual escape speed and the resulting spin of the merged fragment is smaller than the threshold value for rotational fission. When two particles merge, they are replaced by a single spherical particle with the same momentum. Non-merging collisions are modeled as bounces between hard spheres whose post-collision velocities are determined by the amount of dissipation occurring during the collisions. The latter is determined in our simulations by the coefficients of restitution in the tangential and normal directions of the velocity vectors relative to the point of contact (see Richardson, 1994, for details). The values of these coefficients are poorly constrained; we chose to set them both arbitrarily equal to 0.5 (see also Michel et al., 2002).

4. The Eunomia family

We use the Eunomia family formation event as a typical example of the breakup of a large object in the barely disruptive impact regime. The largest member of the observed family contains approximately 70% of the original mass of the parent body, whose diameter is estimated to have been 284 km (Tanga et al., 1999). This body was represented by 2×10^5 SPH particles. The bulk density was set to 2.7 g/cm^3 for the monolithic parent body. The pre-shattered model contained 50 fragments, a fraction of damaged mass at the interfaces equal to 0.17, and a void fraction of 0.075, which results in a somewhat lower bulk density of 2.5 g/cm^3. The mass fraction in the smallest initial fragment turned out to be 6.5×10^{-3} and that in the largest fragment 3.2×10^{-2}.

In order to test the sensitivity of the outcome to the impact geometry, we considered a projectile, also pre-shattered, impacting either "head-on" or with an angle of incidence of 45°. Note that for a specified mass of the largest remnant, the projectile's size depends on the impact geometry, because for a given impact energy, a "head-on" impact is more disruptive than a grazing one. For both kinds of parent bodies, we computed the fragmentation phase using the SPH hydrocode and found that in all cases the target was totally pulverized down to the resolution limit, which corresponds to a fragment radius of 2.38 km. We then computed the gravitational phase using the parallel N-body code `pkdgrav` over 11 days of simulated time.

Tables 1 and 2 summarize the results obtained for the largest remnant's mass and speed, respectively. The mean ejection speed of fragments larger than the resolution limit (i.e., those that underwent at least one re-accumulation) is also indicated. From Table 1, it can be seen that roughly equivalent largest remnants are obtained even though a significantly lower impact energy was necessary in the case of a pre-shattered parent body. In other words, all other things being equal, pre-shattered bodies are easier to disrupt than

Table 1
Summary of simulation parameters

Family	θ (°)	R_p (km)	Q (erg/g)	M_{lr}/M_{pb}
Eunomia M	0	28.90	1.05×10^9	0.67
Eunomia S	0	27.50	9.06×10^8	0.72
Eunomia M	45	38.00	2.39×10^9	0.66
Eunomia S	45	33.80	1.68×10^9	0.70
Karin M	0	1.35	1.57×10^8	0.52
Karin S	0	1.03	6.97×10^7	0.47
Karin M	45	1.65	2.87×10^8	0.50
Karin S	45	1.21	1.13×10^8	0.51
Karin R	45	1.50	2.16×10^8	0.49
Koronis M	0	15.50	2.15×10^9	0.08
Koronis S	0	10.75	7.17×10^8	0.05
Koronis M	45	18.70	3.77×10^9	0.05
Koronis S	45	13.90	1.55×10^9	0.07

M and S refer to either a monolithic parent body or a pre-shattered parent body, respectively. The projectile's angle of incidence is θ. Results of simulations by Michel et al. (2003) for the Karin family are also included here; the label R indicates a rubble-pile parent body (see the last paragraph of Section 2). Impact conditions are defined by the specific impact energy $Q =$ (projectile kinetic energy)/(target mass), which involves the projectile's radius R_p. M_{lr}/M_{pb} is the resulting mass ratio of the largest remnant to the parent body.

Table 2
Properties of fragment ejection speeds

Family	θ (°)	$V_{\rm lr}$	$\langle V \rangle$	$V_{\rm med}$	$V_{\rm max}$	$f_{\rm KE}$
Eunomia M	0	1	120	92	854	0.211
Eunomia S	0	22	210	186	918	0.258
Eunomia M	45	44	128	92	1724	0.200
Eunomia S	45	33	194	170	998	0.229
Karin M	0	6	18	10	362	0.172
Karin S	0	4	14	11	143	0.163
Karin M	45	9	19	14	157	0.173
Karin S	45	4	15	12	283	0.171
Karin R	45	5	14	12	202	0.165
Koronis M	0	31	82	42	789	0.296
Koronis S	0	23	118	101	792	0.283
Koronis M	45	80	105	90	1396	0.228
Koronis S	45	39	119	100	823	0.252

Family labels are the same as in Table 1. Speeds are given in m/s. $V_{\rm lr}$ is the largest remnant ejection speed. $\langle V \rangle$ is the average speed of fragments which underwent at least one reaccumulation event, while $V_{\rm med}$ and $V_{\rm max}$ are, respectively, their median and maximum speeds. The parameter $f_{\rm KE}$ is the so-called *anelasticity parameter*. Here we define it by the ratio of the sum of the kinetic energy of all fragments, including the smallest ones, to the projectile's kinetic energy (see Section 6.3 for a discussion).

Table 3
Computed mass ratios showing the differences between the fragment masses obtained from the disruption of different parent body models

Family	θ (°)	$M_{\rm lr}/M_{\rm pb}$	$\sum_{i=2}^{5} M_i/M_{\rm lr}$
Eunomia M	0	0.67	0.015
Eunomia S	0	0.72	0.038
Eunomia M	45	0.66	0.003
Eunomia S	45	0.70	0.038
Karin M	0	0.52	0.0007
Karin S	0	0.47	0.1261
Karin M	45	0.50	0.0100
Karin S	45	0.51	0.0507
Karin R	45	0.49	0.0470
Koronis M	0	0.08	0.114
Koronis S	0	0.05	2.518
Koronis M	45	0.05	0.308
Koronis S	45	0.07	2.699

$\sum_{i=2}^{5} M_i = M_2 + M_3 + M_4 + M_5$ is the sum of the masses of the second- to fifth-largest fragments.

monolithic ones. A similar conclusion was already reached by Michel et al. (2003) in their studies of the Karin family, which took place in an intermediate impact energy regime.

The size distributions of fragments from a monolithic and a pre-shattered parent body together with the real family members are presented in Figs. 1 and 2. Clearly, the two different internal structure models lead to quite different fragment distributions, the pre-shattered target being in better agreement with observations, as far as the number of large fragments is concerned. More precisely, the disruption of such a parent body leads to the formation of many more large fragments through gravitational re-accumulation, so that the distribution as a whole appears quite continuous. On the other hand, the break-up of a monolithic parent body also produces a fairly large number of re-accumulated fragments, but the outcome is characterized by a very large fragment followed by many much smaller aggregates. This characteristic does not depend much on the impact geometry (angle of incidence of the projectile) nor, as we shall see later, on the impact energy. Quantitatively, this can also be seen in Table 3, where the total mass contained in the second- to fifth-largest fragments normalized to the mass of the largest remnant is compared between the two cases (see also Section 6 for a more detailed discussion). Considering smaller real family members, their size distribution lies

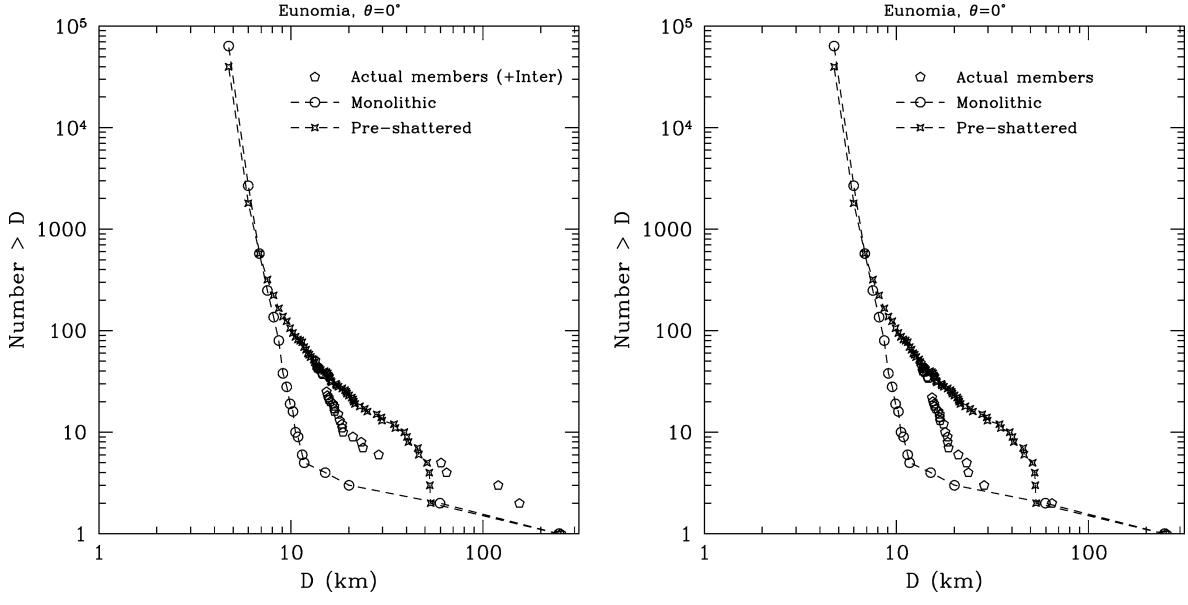

Fig. 1. Cumulative diameter distributions in log-log plots for the fragments of the simulated Eunomia families obtained with a projectile colliding "head-on." Different symbols are used to distinguish between different parent body models. The plot on the left also shows the real members (Tanga et al., 1999) while on the right the potential interlopers (2nd and 3rd largest members) have been removed from the actual distribution.

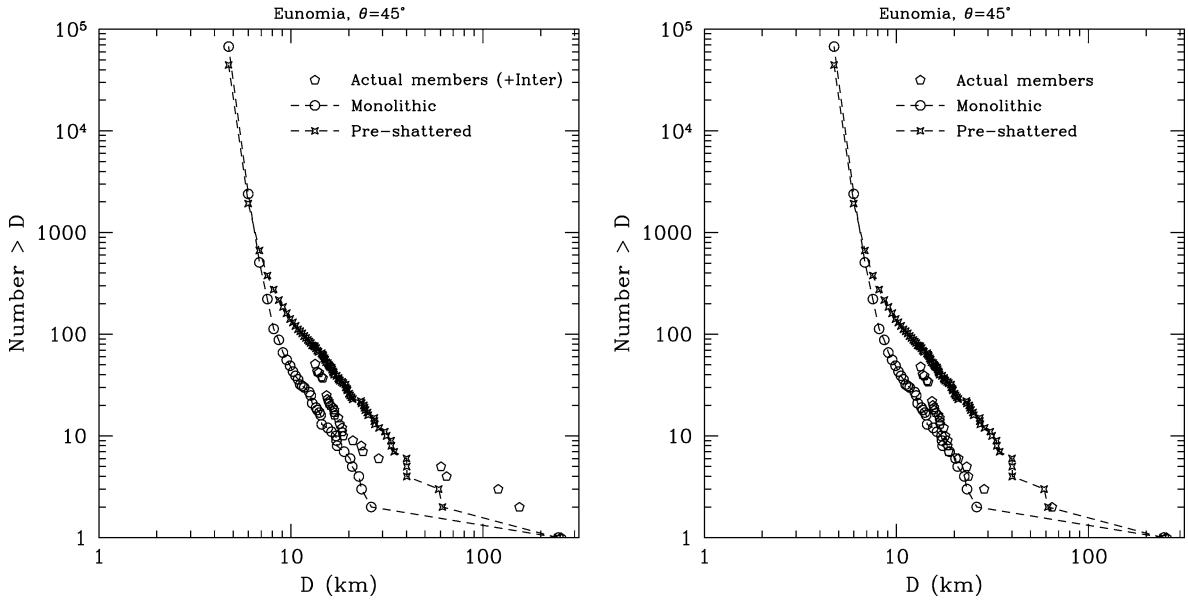

Fig. 2. Same as Fig. 1 obtained using a projectile impacting with an angle of incidence θ equal to 45°.

between the ones produced by both models. Assuming that the Eunomia family was produced at least a few hundreds millions years ago, collisional erosion might still explain, qualitatively at least, the observed size distribution originating from the one produced by a pre-shattered parent body, whereas it is more difficult to explain it originating from the other model. Therefore, the size distribution of fragments from a pre-shattered target, taken as a whole, appears more consistant with the actual family, accounting for its possible collisional history.

It is interesting to note that the two large well-known interlopers (Lazzaro et al., 2001) in the real family can be clearly identified from a comparison between the simulated and real family size distribution (see Figs. 1 and 2). This opens the possibility of using numerical simulations of family formation to help select good candidates for spectral observations in order to check from their taxonomic type if they are actual family members.

The internal structure of the parent body also influences, although less dramatically, the fragments' ejection speeds. While a pre-shattered body does not necessarily yield the highest ejection speed, it systematically leads to higher mean and median speeds (see Table 2). This suggests that the collisional process in a pre-shattered parent body is more efficient in transferring kinetic energy to fragments. A priori, we might expect that the presence of damaged zones in a parent body decreases the efficiency of the shock wave propagation and thus enhances dissipative effects. In reality, the opposite happens. We explain this somewhat surprising result by the fact that in our model of pre-shattered targets there is no real discontinuity or impedance mismatch for the shock wave between fragments and cracks, since:

(i) both are modeled with the same material; and
(ii) void space is small.

On the other hand, rarefaction waves which actually induce fracture inside the parent body cannot cross cracks since these are completely damaged regions. Hence, momentum can be imparted to fragments without having to wait until the rarefaction wave has induced total failure.

This correlation between internal structure of the parent body and mean speed of fragments, while existing in the Eunomia and Koronis families (see below), seems absent in the Karin family. We explain this by the fact that in the latter case the parent body is much smaller and hence requires less specific energy to disrupt. Since the impact speed has been fixed at 5 km/s, this translates into a proportionally smaller projectile. As shown by Benz and Asphaug (1999), the efficiency of momentum transfer is directly related to the ratio between projectile and target radius. This effect results in our case in very small ejection speeds which do not allow us to distinguish between internal structure models.

Another way to analyze the difference in speeds is to make a plot of fragment size as a function of ejection speed. Figures 3 and 4 show these plots for both parent bodies in the case of a 45° impact. It is apparent that in a given size range, ejection speeds of fragments are generally higher for the pre-shattered parent body. These higher ejection speeds are an important property that seems to be systematic, as we will see in the next case.

5. The Koronis family

The highly catastrophic regime is illustrated by the formation of the Koronis family. Its largest remnant contains $\sim 5\%$ of the estimated parent body mass (Tanga et al., 1999). The parent body, 120 km in diameter, was represented by 2×10^5 SPH particles. The bulk density was set to 2.7 g/cm^3 for the monolithic parent body. The pre-shattered model con-

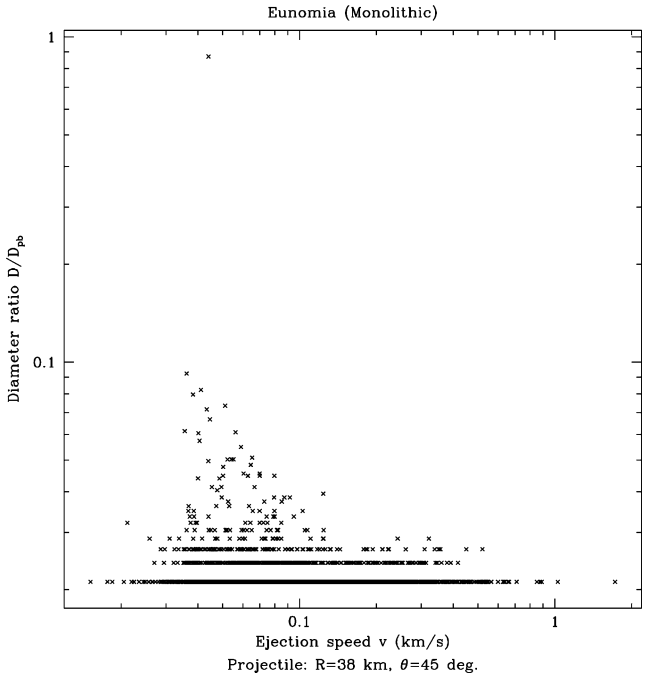

Fig. 3. Fragment diameter D (normalized to that of the parent body $D_{\rm pb}$) vs. ejection speed in a log-log plot obtained from the monolithic Eunomia parent body simulation using a projectile impacting with an angle of incidence $\theta = 45°$. Only fragments with size above the resolution limit (i.e., those that underwent at least one reaccumulation event) are shown here.

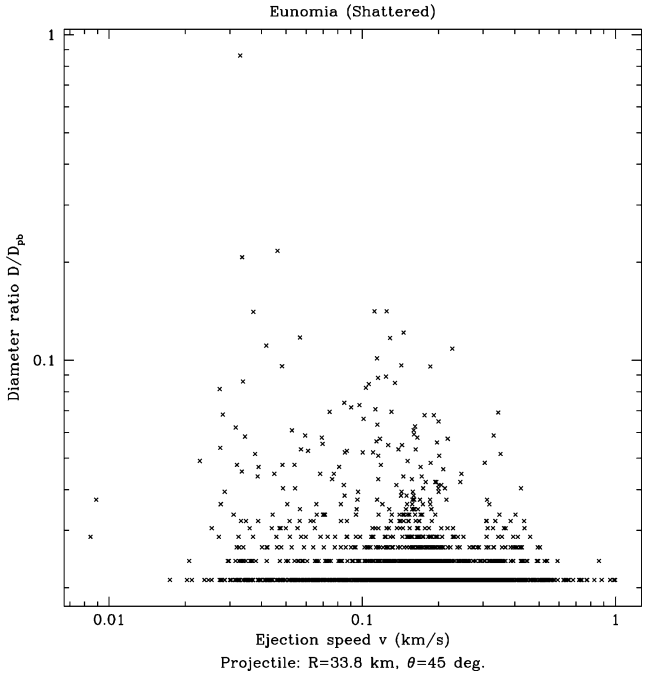

Fig. 4. Same as Fig. 3 but for a pre-shattered Eunomia parent body.

tained 50 fragments, a fraction of damaged mass at the interfaces equal to 0.17, and a void fraction of 0.075, which results in a somewhat lower bulk density of 2.5 g/cm^3. The mass fraction in the smallest fragment turned out to be 5.6×10^{-3} and that in the largest fragment 3.2×10^{-2}. The projectile was also pre-shattered.

As for Eunomia, we find that the fragmentation phase leads to a total pulverization of both kinds of parent body down to the resolution limit, which corresponds to a fragment radius of 1 km. The gravitational phase computed with the N-body code over 23 days of simulated time led to many re-accumulation events, giving rise to two different fragment size distributions (see Fig. 5). Again, the one obtained using a pre-shattered parent body contains a much greater number of large fragments.

Interestingly, the two simulations starting with a pre-shattered parent body lead to the formation of four largest fragments of nearly equal size. This peculiar characteristic which is shared by the real family has been a source of controversy. Indeed, catastrophic disruption and the subsequent gravitational re-accumulation were, until now, not believed to be able to produce a fragment size distribution featuring several large, nearly equal-size bodies. Therefore, alternative scenarios to explain the Koronis family have been proposed involving the post-breakup collisional evolution of the asteroid family. One of them invokes a secondary breakup of the original largest remnant, which would then have been larger than the current one (Marzari et al., 1995). In that case, the original parent body of the Koronis family should also have been larger than the one estimated from the current size distribution assuming no secondary breakup.

However, Ryan et al. (1991) found in their laboratory experiments of impacts on rubble piles that the occurrence of four to seven large fragments having masses within a factor of two of each other is not unusual. From these results, Marzari et al. (1995) speculated that the presence of these large, nearly equal-size fragments in the Koronis family reflects a composite structure of the parent body. While we reach a similar conclusion, our results have a different meaning since they are obtained in the gravitational regime in which fragments are aggregates and not intact bodies. Hence, we have demonstrated for the first time that these fragments can actually be produced by the original family formation event and that no subsequent mechanism requiring a revision of the family's history is needed to explain their presence.

In Fig. 5 we also compare the overall size distribution of family members obtained in our simulations to the real family down to the completeness limit. It is apparent that while in the pre-shattered case the largest fragments show an excellent agreement, the simulated distributions are systematically shallower at smaller sizes. Since collisional evolution cannot steepen such a distribution, we have no good explanation for this difference except to note that no particular effort was made to match in detail this distribution. We used only the largest fragment to determine the collision parameters. We cannot exclude that shape or rotation could also affect the slope of the size distribution.

As we did for the Karin family (Michel et al., 2003), we converted the ejection velocities of the fragments of the Koronis family from our simulations into orbital elements using Gauss' formulae and compared their spreading with

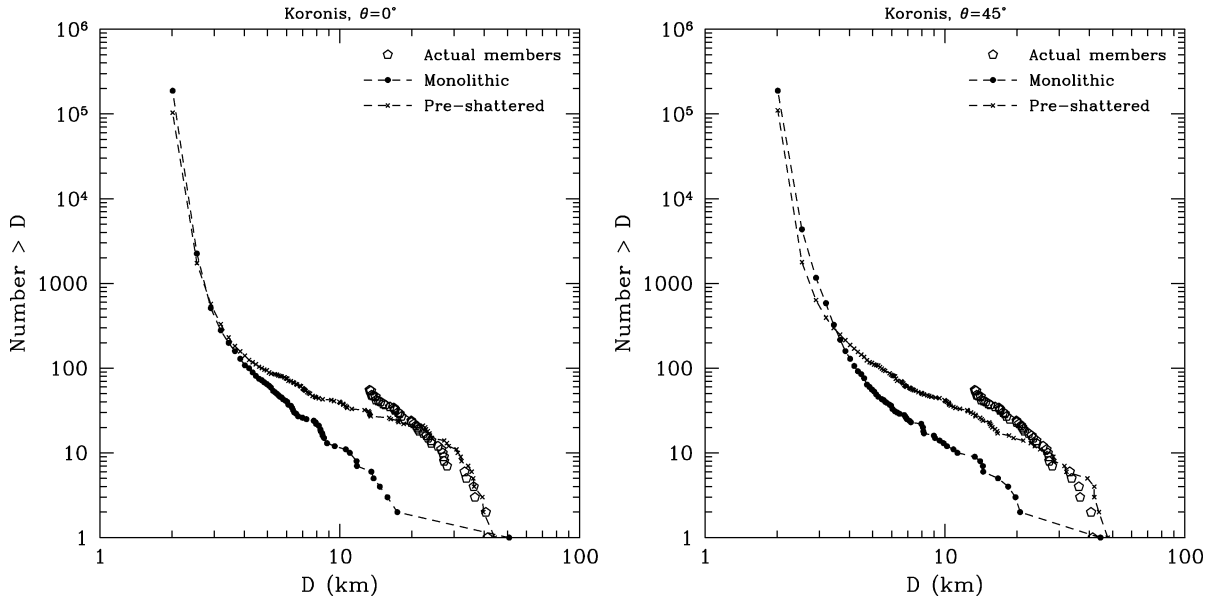

Fig. 5. Cumulative diameter distributions in log-log plots for the fragments of the simulated Koronis families. The plot on the left was obtained with a projectile colliding "head-on," whereas an impact with an angle of incidence θ equal to 45° gave rise to that on the right. Different symbols are used to distinguish between parent body models. The plots also show the estimated sizes of the actual members down to the completeness limit (Tanga et al., 1999). Note that the simulations using a pre-shattered target reproduce the four nearly identical largest members.

that of real family members in proper element space. Figures 6 and 7 show the results for the monolithic and the pre-shattered parent bodies. Our arbitrary choice of values for the orbital semimajor axis and inclination of the projectile (the eccentricity being derived from the Tisserand constant) as well as the true anomaly and argument of perihelion of the parent body at the instant of impact, are indicated on the plots. It is evident that the spreading of the family members obtained from a pre-shattered target is in much better agreement with observations. However, one characteristic of the real members that is not reproduced with either model is the shape of the eccentricity distribution at large semimajor-axis. Different choices of free parameters (e.g., true anomaly of the parent body) can change the shape but not sufficiently to reproduce the observed eccentricity distribution. However, dynamical diffusion due to efficient high-order resonances has been shown to be able to account for such a shape (Bottke et al., 2001). Interestingly, fragments from a pre-shattered parent body show a spread in semimajor axis similar to the one of the real family. Hence, it is not necessary to invoke the Yarkovsky effect to explain the observed spread. However, the apparently non-random orientation of the spin vectors of large Koronis family members (Vokrouhlický et al., 2003) may still require that the family be old in order to leave enough time for the thermal torques to align them.

6. Internal structure and outcome properties

In this section, we discuss different collisional outcome characteristics and their dependence upon the internal structure of the parent body. In particular, we look at the size distribution, the location inside the parent body of the material forming the largest gravitationally re-accumulated aggregates, the efficiency with which the projectile's kinetic energy is distributed among the family members, and the characteristics of the numerous satellites formed.

6.1. Number of large fragments

As we have already noted, the most striking difference in collisional outcomes is related to the fragment size distribution, which is systematically much more continuous when a pre-shattered parent body is considered. To quantify this property, we have computed, for each case, the ratio $\sum_{i=2}^{5} M_i/M_{\rm lr}$ of the mass contained in the second- (M_2) to fifth- (M_5) largest fragments to that of the largest one ($M_{\rm lr}$). As can be seen in Table 3, this ratio, which is independent of the size of the parent body, appears systematically much higher for a pre-shattered parent body, with a trend toward a systematic increase of its value with the degree of disruption (see Fig. 8).

Assuming that our limited analysis is sufficiently general, in a highly catastrophic regime (represented here by the Koronis family formation), Table 3 suggests that the parent body was monolithic if the mass ratio $\sum_{i=2}^{5} M_i/M_{\rm lr}$ is in the ~ 0.1 range. In the intermediate regime (represented by the Karin family formation), values smaller than ~ 0.01 would imply such a structure for the parent body. Finally, in the barely disruptive regime (represented by the Eunomia family formation) this ratio must be smaller than ~ 0.02 for such a body.

We can attempt to apply this criterion to other S-type asteroid families (recall that we used basalt bodies). For in-

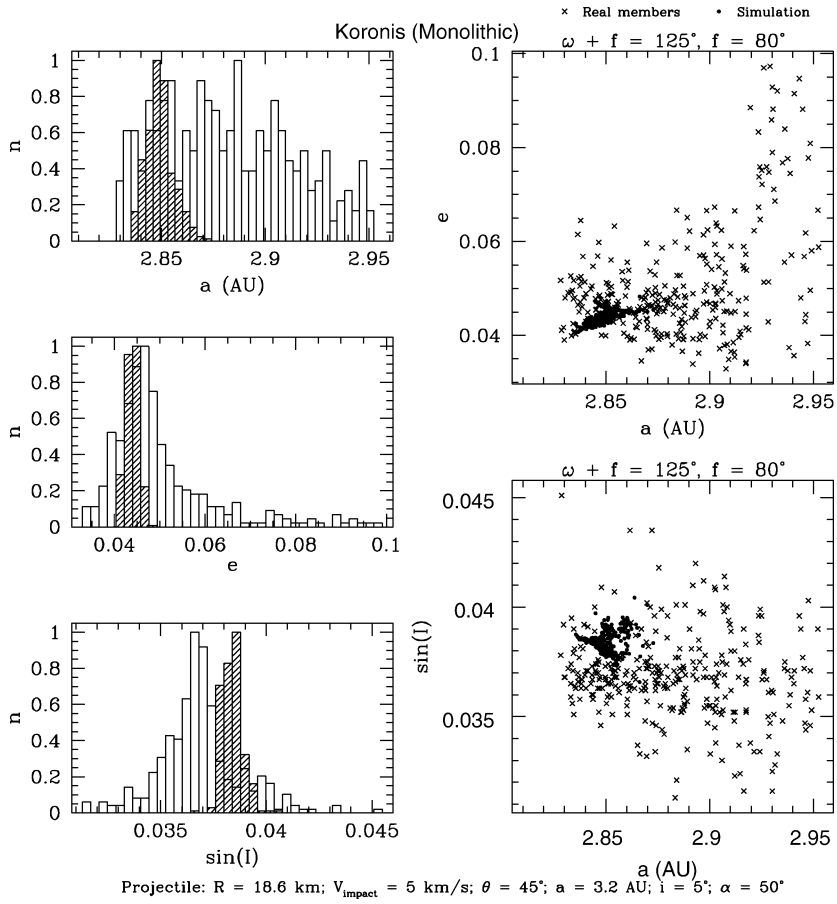

Fig. 6. (Left) From top to bottom, histograms of the proper semimajor axis, eccentricity, and sine of inclination for both the real members of the Koronis family (open bars) and the simulated family (filled bars) from the disruption of a monolithic parent body. For the latter, the orbital elements are computed from Gauss' equations, assuming a main-belt-like orbit of the projectile (its semimajor axis a and inclination i are indicated at the bottom of the plot; its eccentricity can be derived from the formula for the Tisserand constant). The values of the parent body's true anomaly at impact f and its sum with the argument of perihelion $\omega + f$ are assumed to be equal to, respectively, 80° and 125°. The histograms are individually normalized to the number of objects in the most populated bin. (Right) Distributions in the eccentricity vs. semimajor axis plane (top) and in the sine of inclination vs. semimajor axis plane (bottom) of the real members and of the simulated family.

stance, the Maria family, whose parent body diameter is estimated at 130 km and whose mass ratio $M_{\rm lr}/M_{\rm pb}$ is equal to 0.05 (Tanga et al., 1999), has a ratio $\sum_{i=2}^{5} M_i/M_{\rm lr}$ equal to 2.9, indicating a pre-shattered parent body. The same holds true for the Eos family, for which this ratio is equal to 1.1, with a parent body 218 km in diameter, and $M_{\rm lr}/M_{\rm pb} = 0.11$ (Tanga et al., 1999). Finally, this exercise applied to the Flora family gives a value of 0.13 for a parent body diameter equal to 164 km and $M_{\rm lr}/M_{\rm pb} = 0.57$ (Tanga et al., 1999). Thus, our simple criterion, if true, indicates that all these families have originated from pre-shattered asteroids. This is consistent with the idea that large asteroids get battered over time by small impacts before undergoing a dispersal/family-forming event.

6.2. Initial positions of particles forming the largest fragments

It is interesting to trace back, at least for some of the largest fragments, the original positions within the parent body of the particles that end up forming these aggregates. If re-accumulation is a random process, we expect the particles of a given large fragment to originate from uncorrelated regions within the parent body. Conversely, if the initial velocity field imposed by the fragmentation process determines the re-accumulation phase, the particles belonging to the same fragment should originate from well defined areas inside the parent body. In addition, the position and extent of these regions will provide indications about the mixing occurring as a result of the re-accumulation process.

In Fig. 9 we traced the particles belonging to the three largest fragments of the Koronis family (45° impact) back to their original positions inside the parent body. In such a highly catastrophic event, the re-accumulation process lasts up to several days, much longer than for a barely disruptive event, and gives rise to many gravitational encounters. Therefore, this kind of event may well lose the memory of the initial velocity field. Nevertheless, even in this case, particles are found to originate from well clustered regions within the parent body, indicating that re-accumulation is

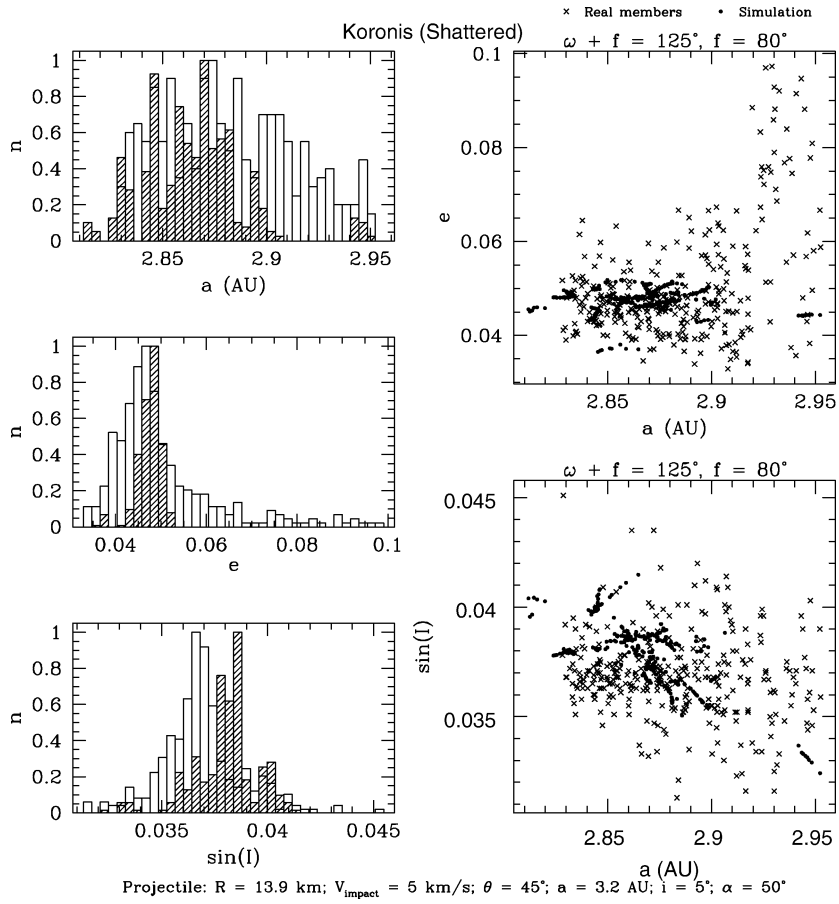

Fig. 7. Same as Fig. 6 for the disruption of a pre-shattered parent body.

definitely not a random process. Interestingly, the position of the cluster depends greatly on the internal properties of the parent body. The largest remnant of our pre-shattered model involves particles that were initially located between the core and the region antipodal to the impact point. Conversely, in the monolithic parent body, those particles were initially much more clustered in the core region, with no particles originating from the antipode. This difference also holds true for the next largest fragments.

In summary, our results indicate that the velocity field arising from fragmentation has a major influence on the reaccumulation process. Particles that eventually belong to a given fragment originate from the same region inside the parent body. However, this location (as well as its extent, which determines the degree of mixing of the fragments) depends also on the parent body's internal properties in a complex way. Since this may be particularly important for differentiated bodies, we plan to investigate this in more detail in future studies.

6.3. *Kinetic energy partitioning f_{KE} and ejection speeds*

We can use our simulations to investigate the meaning of the parameter f_{KE}, defined in the literature as the fraction of the projectile kinetic energy that is transferred to all the fragments.

Computing f_{KE} from all the fragments down to the resolution limit of a single particle, we find in all cases a value of order 0.1 regardless of structure or geometry (Table 2). This clearly indicates that f_{KE} is not a good indicator of internal structure.

It is important to realize that determining the actual value of f_{KE} may actually be tricky since, while independent of internal structure when considering all fragments, it is a strong function of target structure if only a subset of fragments is considered. To illustrate this point, we plot in Fig. 10 the value of f_{KE} obtained as a function of fractional mass starting with the largest fragments for both models of the Koronis parent body. Strikingly, f_{KE} varies in both cases by more than two orders of magnitude. Using only the large fragment end of the distribution yields values of order 0.001 regardless of the structure model, while using all fragments yields values of order 0.2. However, with intermediate amounts of the fractional mass, we obtain f_{KE} values that depend strongly upon initial structure. For example, at 50% fractional mass, $f_{KE} = 0.1$ in the case of a monolithic target while $f_{KE} = 0.01$ in the case of a pre-shattered target. This is because f_{KE} values computed for a given fractional mass involve many more smaller fragments (which tend to have higher speeds) in the monolithic case than in the pre-shattered case. Thus, a higher f_{KE} value does not imply that fragments of a given mass have higher speeds, but simply that more ki-

netic energy has been given to the material used to compute f_{KE}. Conversely, identical values of f_{KE} imply that the same amount of kinetic energy has been imparted to a number of large fragments in the pre-shattered case and to a larger number of smaller fragments in the monolithic case.

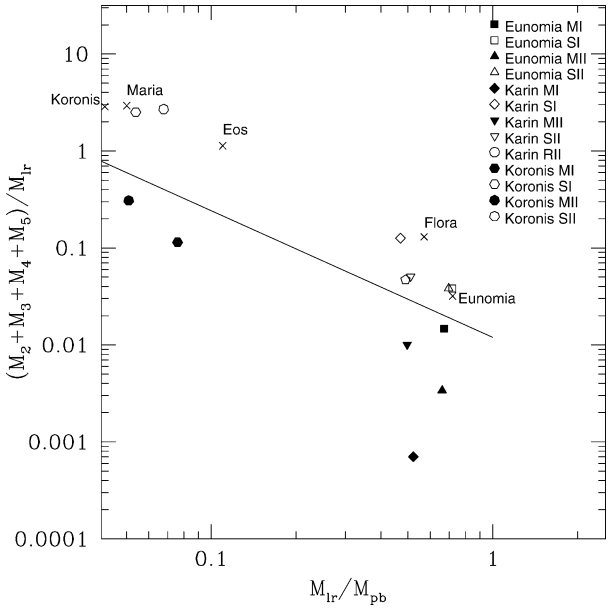

Fig. 8. Plot of the ratio of the sum of the mass of the second- to fifth-largest fragments (M_2, M_3, M_4, M_5) over M_{lr} vs. M_{lr}/M_{pb}, obtained from the different simulations of the Eunomia, Karin, and Koronis family formations. Family labels are identical to the ones used in the tables. Filled and open symbols are used for monolithic (M) and pre-shattered (S) parent bodies, respectively. Polygons with an even or odd number of sides correspond to impact with a projectile angle of incidence equal to 0° (I) or 45° (II), respectively. Outcomes obtained from pre-shattered parent bodies are systematically well above those obtained from monolithic parent bodies in all impact energy regimes. A straight line can be drawn which separates the two models. Data from five observed families are also indicated.

This implies, for example, that f_{KE} values determined from laboratory experiments, in which the speeds of only a fraction of the fragments can be determined, are misleading and do not represent the true value of f_{KE} when computed over all the fragments. The same remark obviously applies to asteroid families for which only members above the detection threshold are used in the computation of f_{KE}.

Power law relations between fragment masses and speeds are often used in the computation of the collisional evolution of a population of small objects (see e.g., Davis et al., 2003). Our simulations show no such simple relation but rather a wide spread of ejection speeds for fragments of a given mass (see Figs. 3 and 4), even though a trend exists that smaller fragments tend to have larger ejection speeds.

6.4. Formation of asteroid satellites

Table 4 indicates the number of satellites orbiting the largest remnant at the end of each simulation. As Michel et al. (2001, 2002) already found, a great number of largest-remnant satellites are generally produced during a collisional disruption in all impact energy regimes. This process is investigated in detail in the case of monolithic parent bodies by Durda et al. (2003). We find that the number of satellites produced does not provide a diagnostic of the parent body internal structure, since both kinds of parent bodies (monolithic and pre-shattered) give rise to a large number of satellites whose characteristics are indistinguishable. Satellite capture depends on individual fragment trajectories and is a very sensitive process since interactions must avoid leading to collision or escape. Therefore, it is not so surprising

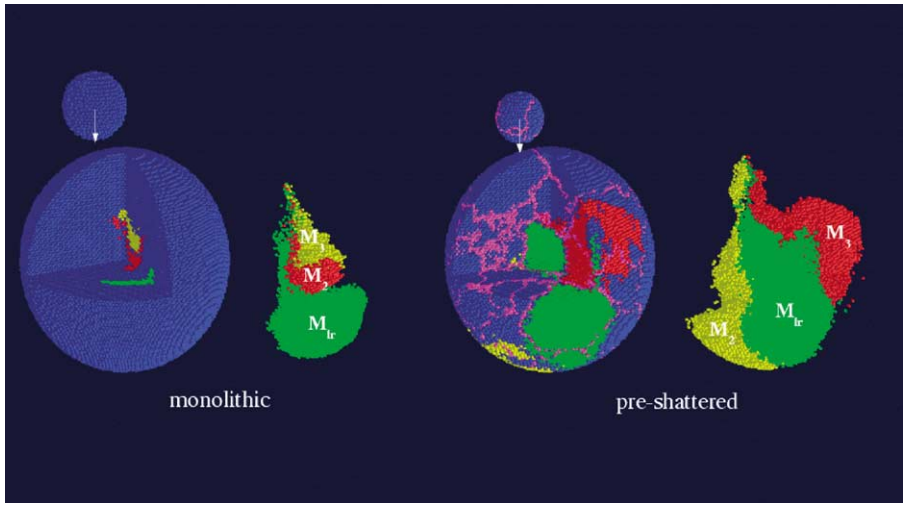

Fig. 9. Initial location within the parent body ((left) monolithic; (right) pre-shattered) of the particles ending up forming the three largest fragments of the Koronis family (45° impact angle). M_{lr} is shown in green, and the second- (M_2) and third- (M_3) largest fragments are shown in yellow and in red, respectively. The initial damaged zones defining the fragments within the pre-shattered parent body are visible as pink lines. For each model we show two 3D images of the particles eventually making up these three fragments: (1) inside the parent body (in blue) from which 1/8th was cut out and (2) without the remainder of the parent body.

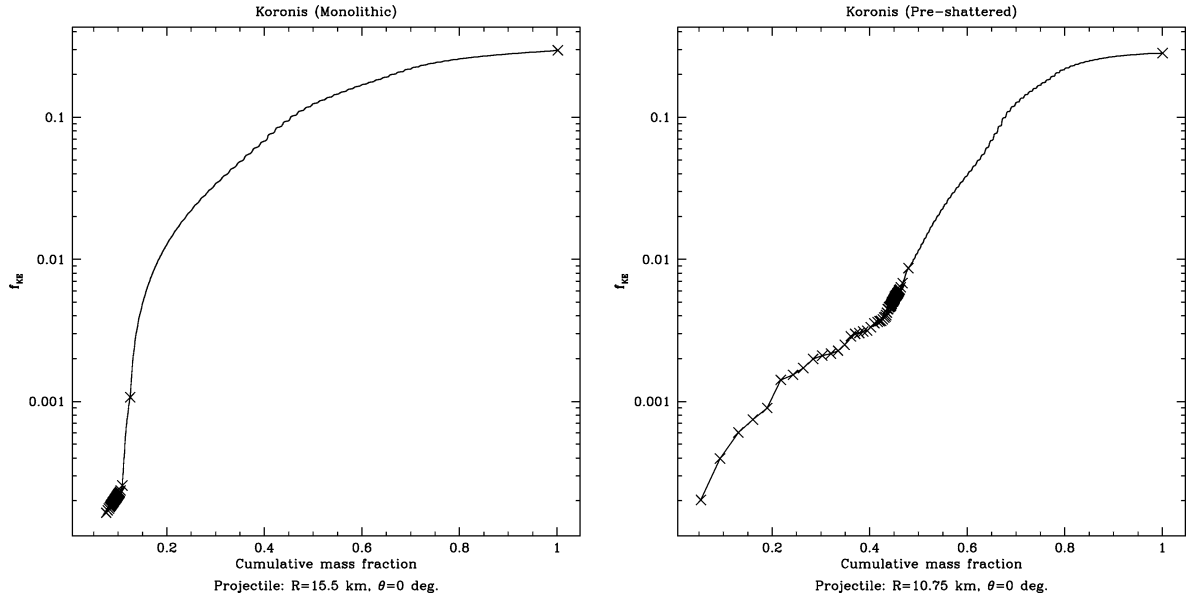

Fig. 10. Two plots from the simulations of the Koronis family formation showing the values of f_{KE} (anelasticity parameter) as a function of the fractional mass used in its computation. Between crosses, fragments have identical mass. The impact angle was equal to 0° and the parent body was either monolithic (left) or pre-shattered (right).

Table 4
Number of satellites of the largest remnant at the end of each simulation with the different parent body models

Family	θ (°)	Nb total	Nb total, $Q < R_H$	Nb, $R > R_{\min}$	Nb, $R > R_{\min}$, $Q < R_H$	M_{ls}/M_{prim}
Eunomia M	0	23 (0.04)	19 (0.03)	2 (0.07)	2 (0.07)	3.5×10^{-5}
Eunomia S	0	181 (0.45)	180 (0.45)	19 (1.05)	19 (1.05)	1.3×10^{-4}
Eunomia M	45	628 (0.93)	608 (0.90)	58 (2.42)	57 (2.38)	3.5×10^{-4}
Eunomia S	45	295 (0.66)	292 (0.66)	16 (0.83)	16 (0.83)	6.6×10^{-5}
Karin M	0	17 (0.02)	13 (0.01)	5 (0.51)	5 (0.51)	1.5×10^{-4}
Karin S	0	705 (0.80)	681 (0.77)	50 (2.31)	50 (2.31)	2.5×10^{-3}
Karin M	45	486 (0.46)	463 (0.44)	36 (4.34)	35 (4.22)	7.2×10^{-3}
Karin S	45	288 (0.34)	276 (0.32)	24 (1.04)	23 (1.00)	1.7×10^{-4}
Karin R	45	345 (0.61)	340 (0.60)	9 (1.68)	9 (1.68)	3.2×10^{-3}
Koronis M	0	183 (0.10)	175 (0.09)	14 (0.62)	13 (0.58)	1.2×10^{-4}
Koronis S	0	386 (0.37)	378 (0.36)	12 (0.69)	12 (0.69)	1.2×10^{-3}
Koronis M	45	505 (0.27)	480 (0.26)	45 (1.03)	44 (1.01)	7.4×10^{-4}
Koronis S	45	285 (0.26)	284 (0.26)	8 (0.45)	8 (0.45)	5.3×10^{-4}

θ is the impact angle. The fourth column indicates the total number of satellites with orbits entirely inside the Hill's radius of their primary, located at a heliocentric distance of 2.644 AU for Eunomia and 2.866 AU for Karin and Koronis. The corresponding percentage of the total number of fragments at the same instant is indicated in parentheses. Q is the maximum distance to the primary of the satellite along its orbit. In the columns with $R > R_{\min}$, only objects with radius greater than the minimum value $R_{\min}$ imposed by the resolution of our simulations have been considered. In this case, the corresponding percentage of the total number of fragments which underwent at least one reaccumulation is indicated in parentheses. The last column gives the mass ratio of the largest satellite to the primary.

that, due to the somewhat chaotic nature of the process, the initial ejection velocity field does not tightly constrain the satellite capture efficiency, even though the internal structure of the parent body does affect the global properties of the ejection velocity field and hence the reaccumulation process and fragment properties.

We note that head-on impacts with a monolithic parent body seem to generate a smaller number of largest-remnant satellites than head-on impacts with a pre-shattered parent body. The opposite is found for projectiles impacting with a 45° angle of incidence. Also, with monolithic parent bodies, head-on impacts produce generally fewer largest-remnant satellites than 45° impacts. With pre-shattered parent bodies, the number of satellites generated from oblique impacts is greater than for head-on impacts, but only for those satellites which underwent at least one reaccumulation. The origin of these systematic differences is not obvious and would require a deeper analysis of satellite formation based on a greater number of simulations, which is beyond the scope of this paper.

7. Conclusion

This work represents another step in our understanding of collisional processes involving asteroids. In Michel et al. (2002), we concluded that using a monolithic target may not be realistic, since prior to a dispersing event, asteroids as large as family parent bodies are likely to have already been battered by numerous previous small impacts (Asphaug et al., 1998). Here, we constructed different models of such pre-shattered parent bodies and simulated their disruption. The results confirm those of Michel et al. (2003) for the particular case of the young Karin family and show that the breakup of a pre-shattered parent body generally leads to outcome properties in better agreement with asteroid family properties. In particular, the obtained fragment size distribution is almost continuous in collisions involving a pre-shattered parent body while it lacks intermediate size fragments in the monolithic case. Thus, we tentatively propose a parent body internal structure indicator which consists of the mass ratio between the sum of the second- to fifth-largest fragment and the largest fragment (see Table 3).

Since real family members have continuous size distributions and only pre-shattered parent bodies seem capable of yielding such distributions, we conclude that before being disrupted, most asteroid family parent bodies must have been extensively fractured. Note that this scenario is in good agreement with the current view of the history of the asteroid belt. We can also compute the expected family formation frequency using the results of our still relatively simple collision simulations and rough estimates of projectile and target numbers. We obtain that one Koronis family is expected to form every 1 Gyr, one Eunomia family every 1.2 Gyr and one Karin family every 10 Myr (F. Marzari, private communication), again in good agreement with accepted ages.

Another important result of this study is that the impact energy required to achieve a given degree of disruption is a function of internal structure. Even within pre-shattered targets variations exist depending upon the presence or absence of large void spaces which influence the efficiency at which kinetic energy is distributed throughout the target and ultimately to the fragments. We plan to investigate this further, together with the effect of smaller-scale porosity, in a forthcoming paper.

In light of the present results, we believe that any estimate of the impact energy needed to create a given degree of disruption requires a rather good knowledge of the internal structure of the target. This conclusion has many implications in a wide range of studies. For instance, it indicates that the internal structure of a body has an influence on its collisional lifetime, which must be taken into account in models of collisional evolution of the asteroid belt and more generally in models of the evolution of planetary systems in all phases. It also appears crucial to have a good knowledge of the internal structures of potentially hazardous asteroids since mitigation strategies aimed at deviating an object on its way to Earth will require an accurate estimate of the impact energy needed to do so.

Acknowledgments

P.M. acknowledges financial support from the Action Thématique Innovante 2001 and the Programme National de Planétologie 2003 of the French Institut National des Sciences de l'Univers (INSU). W.B. acknowledges support from the Swiss National Science Foundation. D.C.R. was supported in part by the NASA Origins of Solar Systems program, grant number NAG5-11722. We are grateful to the ILGA team of the O.C.A. who generously provided access to their 4-processor COMPAQ DEC ALPHA workstation. Simulations were also partly carried out on the *SIVAM II project* 4-processor COMPAQ DEC ALPHA of O.C.A. and on a Beowulf installed by the society *Alineos* and partially financed by both the O.C.A. program *Bonus-Qualité-Recherches* 2001–2002 and the Cassini laboratory (O.C.A.).

References

Asphaug, E., Ostro, S.J., Hudson, R.S., Scheeres, D.J., Benz, W., 1998. Disruption of kilometer-sized asteroids by energetic collisions. Nature 393, 437–440.

Asphaug, E., Ryan, E.V., Zuber, M.T., 2002. Asteroid interiors. In: Bottke Jr., W.F., Cellino, A., Paolicchi, P., Binzel, R.P. (Eds.), Asteroids III. Univ. of Arizona Press, Tucson, pp. 463–484.

Belton, B., Chapman, C.R., Thomas, P., Davies, M., Greenberg, R., Klaasen, K., Byrnes, D., D'Amario, L., Synnott, S., Merline, W., Petit, J.M., Storrs, A., Zellner, B., 1995. The bulk density of Asteroid 243 Ida from Dactyl's orbit. Nature 374, 785–788.

Benz, W., Asphaug, E., 1995. Simulations of brittle solids using smooth particle hydrodynamics. Comput. Phys. Comm. 87, 253–265.

Benz, W., Asphaug, E., 1999. Catastrophic disruptions revisited. Icarus 142, 5–20.

Bottke, W.F., Vokrouhlický, D., Borz, M., Nesvorný, D., Morbidelli, A., 2001. Dynamical spreading of asteroid families via the Yarkovsky effect. Science 294, 1693–1696.

Chapman, C.R., Ryan, E.V., Merline, W.J., Neukum, G., Wagner, R., Thomas, P.C., Veverka, J., Sullivan, R.J., 1996. Cratering on Ida. Icarus 120, 77–86.

Davis, D.R., Durda, D.D., Marzari, F., Campo Bagatin, A., Gil-Hutton, R., 2003. Collisional evolutions of small body populations. In: Bottke Jr., W.F., Cellino, A., Paolicchi, P., Binzel, R.P. (Eds.), Asteroids III. Univ. of Arizona Press, Tucson, pp. 545–558.

Durda, D.D., Bottke, W.F., Enke, B.L., Merline, W.J., Asphaug, E., Richardson, D.C., Leinhardt, Z.M., 2003. The formation of asteroid satellites in large impacts: results from numerical simulations. Icarus. In press.

Lazzaro, D., Mothé-Diniz, T., Carvano, J.M., Angeli, C.A., Betzler, A.S., 2001. The Eunomia family: a visible spectroscopic survey. Icarus 142, 445–453.

Marzari, F., Davis, D., Vanzani, V., 1995. Collisional evolution of asteroid families. Icarus 113, 168–187.

Melosh, J.G., Ryan, E.V., 1997. Asteroids: shattered but not dispersed. Icarus 129, 562–564.

Michel, P., Benz, W., Tanga, P., Richardson, D.C., 2001. Collisions and gravitational reaccumulation: forming asteroid families and satellites. Science 294, 1696–1700.

Michel, P., Benz, W., Tanga, P., Richardson, D.C., 2002. Formation of asteroid families by catastrophic disruption: simulations with fragmentation and gravitational reaccumulation. Icarus 160, 10–23.

Michel, P., Benz, W., Richardson, D.C., 2003. Disruption of fragmented parent bodies as the origin of asteroid families. Nature 421, 608–611.

Nesvorný, D., Bottke, W.F., Dones, L., Levison, H.F., 2002. The recent breakup of an asteroid in the main belt region. Nature 417, 720–722.

Richardson, D.C., 1994. Tree code simulations of planetary rings. Mon. Not. R. Astron. Soc. 269, 493–511.

Richardson, D.C., Quinn, T., Stadel, J., Lake, G., 2000. Direct large-scale N-body simulations of planetesimal dynamics. Icarus 143, 45–59.

Richardson, D.C., Leinhardt, Z.M., Bottke Jr., W.F., Melosh, H.J., Asphaug, E., 2002. Gravitational aggregates: evidence and evolution. In: Bottke Jr., W.F., Cellino, A., Paolicchi, P., Binzel, R.P. (Eds.), Asteroids III. Univ. of Arizona Press, Tucson, pp. 501–515.

Ryan, E.V., Hartman, W.K., Davis, D.R., 1991. Impact experiments. III. Catastrophic fragmentation of aggregate targets and relation to asteroids. Icarus 94, 283–298.

Tanga, P., Cellino, A., Michel, P., Zappalà, V., Paolicchi, P., dell'Oro, A., 1999. On the size distribution of asteroid families: the role of geometry. Icarus 141, 65–78.

Thomas, P.C., Joseph, J., Carcich, B., Clark, B.E., Veverka, J., Miller, J.K., Owen, W., Williams, B., Robinson, M., 2000. The shape of Eros from NEAR imaging data. Icarus 145, 348–350.

Thompson, S.L., Lauson, H.S., 1972. Improvement in the Chart D radiation hydrodynamic code III: revised analytic equation of state. Sandia National Laboratory Report SC-RR-71 0714.

Tillotson, J.H., 1962. Metallic equations of state for hypervelocity impact. General Atomic Report GA-3216, July 1962.

Vokrouhlický, D., Nesvorný, D., Bottke, W.F., 2003. The vector alignment of asteroid spins by thermal torques. Nature 425, 147–151.

Weibull, W.A., 1939. A statistical theory of the strength of material (transl.). Ingvetensk. Akad. Handl. 151, 5–45.